Ergodicity-Breaking in Thermal Biological Electron Transfer? Cytochrome C Revisited

Xiuyun Jiang, Zdenek Futera, and Jochen Blumberger*

Department of Physics and Astronomy and Thomas Young Centre, University College London, London WC1E 6BT, UK.

E-mail: j.blumberger@ucl.ac.uk(J.B.)

Phone: ++44-(0)20-7679-4373. Fax: ++44-(0)20-7679-7145

Abstract

It was recently suggested that certain redox proteins operate in an ergodicity-breaking regime to facilitate biological electron transfer (ET). A signature for this are large variance reorganization free energies (several eVs) but significantly smaller Stokes reorganization free energies due to incomplete protein relaxation on the time scale of the ET event. Here we investigate whether this picture holds for oxidation of cytochrome c in aqueous solution, with various levels of theory including classical molecular dynamics with two additive and one electronically polarizable force field, and QM/MM calculations with the QM region treated by two approaches. Sampling the protein and energy gap dynamics over more than 250 ns, we find no evidence for ergodicity-breaking effects. In particular, the inclusion of electronic polarizability of the heme group at QM/MM levels did not induce non-ergodic effects, contrary to previous reports by Matyushov *et al.* The well-known problem of overestimation of reorganization free energies with additive force fields is cured when the protein and solvent are treated electronically polarizable. Ergodicity-breaking effects may occur in other redox proteins and our results suggest that long simulations, ideally on the ET time scale, with electronically polarizable force fields are required to obtain strong numerical evidence for them.

Introduction

Marcus theory of electron transfer (ET) is arguably one of the most important and impactful accomplishments of modern chemical reaction kinetics.[1,2] It has provided generations of physical chemists, biologists and material scientists with an elegant, robust and perhaps surprisingly accurate framework allowing them to understand, interpret and predict ET processes in very diverse systems ranging from molecular donor-acceptor complexes,[3–6] biomolecules,[7–25] cellular appendages,[25–31] microbial biofilms[32,33] to certain inorganic[34–37] and organic semiconductors[38–41] and electrochemical interfaces.[42–45] The theory is synonymous with the famous pair of intersecting free energy parabolas, one for the initial and one for the final ET electronic state, with ET occuring at the molecular configurations where the two curves cross, commonly referred to as the transition state for ET (see Figure 1A). The elegance of Marcus theory is that the two parabolas and therefore the activation free energy, $\Delta A^{\ddagger}$, is solely determined by just two parameters that can be extracted from experiment or computation, the reaction free energy or driving force ΔA^{0} (i.e. redox potential difference between donor and acceptor) determining their vertical offset and the reorganization free energy λ determining the horizontal offset and curvature, the latter being the same in both states.

All what is needed to arrive at the paradigm of equal-curvature parabolas is to assume that the thermal fluctuations of the ET reaction coordinate, the vertical energy gap ΔE,[46,47] are Gaussian distributed *and* that phase space is sampled according to the Boltzmann distribution on the time scale of the ET reaction (see e.g. Ref.[23] for a formal treatment). It turns out that in the majority of cases these assumptions are fulfilled, which may be rationalized by the central limit theorem even though the energy gap fluctuations due to the molecules of a condensed phase system are not strictly independent. An important consequence that follows is that the horizontal offset of the two curves, defined as twice the Stokes reorganization free energy, λ^{st}, is not independent from their curvature (or force constant $k \propto 1/\lambda^{\mathrm{var}}$, "var" for variance of the corresponding Gaussian fluctuations), but in fact related to it since

$\lambda^{\mathrm{st}} = \lambda^{\mathrm{var}} \equiv \lambda$ is exact for Gaussian fluctuations (see Figure 1A, pair of parabolas in blue). Hence, only one reorganization free energy (λ) appears in Marcus theory.

Yet, exception to the Marcus parabola picture are well known and often attributed to either non-Gaussian energy gap fluctuations[16,23,48–53] or non-Boltzmann (i.e. non-ergodic) sampling of molecular configurations on the ET time scale,[16,23,50,54,55] or both.[16,23,50,55] Non-Gaussian gap fluctuations have been observed for charging of an apolar particle with an unstructured solvation shell,[56] for solutes with a strong difference in electronic polarizability in the initial and final ET states[48,50,57,58] and when oxidation of ions is coupled to a change in first shell coordination number.[49,51,59] For cytochromes in particular, Amadei and co-workers showed that non-Gaussian gap fluctuations can result in a possible discrepancy between the Stokes and the variance reorganization free energy.[52,53] Though, the linear free energy relation equating the vertical free energy gap between the two curves with the energy gap ΔE[23] is still fulfilled in that case, the latter only requiring a Boltzmann distribution of molecular configurations.

Naturally, non-ergodicity is a problem in ultrafast (picosecond) photoexcited ET reactions, e.g. in Photosystem II (PS II).[16,50,57,58] Reorganization and hence activation free energy are strongly overestimated if the energy gap is sampled on time scales longer than the actual ET event.[57,58] Here a self-consistent non-ergodicity correction has been devised where frequency components faster than the ET event are simply removed from the reorganization free energy. This method has been successfully combined with Marcus-Sumi theory[54] to explain the non-exponential population decay observed experimentally in PSII.[50,57,58]

In a series of recent papers, Matyushov *et al.* claims that ergodicity-breaking effects extend well into the regime of thermal biological electron transfer, typically occurring on the microsecond or slower time scales.[16,50,55,60–63] In analogy with glass-forming materials, the often highly charged protein-water interface creates a rugged energy landscape that is not explored ergodically on the time scale of the ET event (see Figure 1B). While the energy gap fluctuations may still be Gaussian and arise, amongst others, from protein motions

necessary to bring the protein from the equilibrium structure of the initial to the equilibrium structure of the final ET state, the rugged energy landscape of the protein-water interface may not allow for this transition to actually occur on the ET time scale (dotted lines in Figure 1B) keeping the solvated protein trapped in some local minimum on the final ET state surface (arrows in Figure 1B). Due to incomplete relaxation, the Stokes reorganization free energy $\lambda^{\rm st}$ is now no longer equal to but smaller than the variance reorganization free energy $\lambda^{\rm var}$, $\lambda^{\rm st} < \lambda^{\rm var}$, amounting to a horizontal shift of the parabolas towards the origin concomitant with a reduction in activation free energy (pair of red parabolas in Figure 1A). Requiring the condition of zero energy gap at the point where the free energy curves cross, it is straightforward to show that in this scenario the activation free energy is still given by the usual Marcus expression but with λ replaced by the smaller reaction reorganization free energy (superscript "r"),[16,55,61–63]

$$\Delta A^{\ddagger,r} = \frac{(\lambda^{\rm r} + \Delta A^0)^2}{4\lambda^{\rm r}} \quad (1)$$

$$\lambda^{\rm r} = \frac{(\lambda^{\rm st})^2}{\lambda^{\rm var}} \quad (2)$$

Using long molecular dynamics (MD) simulations, Matyushov *et al.* reported a strong mismatch between $\lambda^{\rm st}$ and $\lambda^{\rm var}$, with ratios $\kappa_{\rm G} = \lambda^{\rm var}/\lambda^{\rm st} = 7.9$ for the Cu-containing protein plastocyanin,[60] and $\kappa_{\rm G} = 2.3$ for oxidation of cytochrome c (cyt c) at room temperature.[61–63] For plastocyanine the large values for $\lambda^{\rm var}$ were traced back to an incomplete compensation of the gap fluctuations due to the charged/dipolar protein residues at the protein surface by the gap fluctuations due to the dipoles of the water molecules solvating these residues.[55] In cyt c the origin of ergodicity-breaking was of a more subtle nature: it was traced back to the strong electronic polarizability of the heme-c cofactor in oxidized and reduced states and it disappeared when the heme c cofactor was treated non-polarizable.[61]

The existence of ergodicity-breaking effects would profoundly change our traditional understanding of thermally activated biological ET reactions. It would mean that certain

biological ET reactions occur on physiological time scales because the protein does not have sufficient time to convert between the (global) equilibrium structures of initial and final ET states, and if it had, ET would be too slow in these proteins to support biological function.

In contrast to the above, MD simulations carried out in our group on similar heme and Cu-containing redox proteins have so far not given any evidence for ergodicity-breaking effects: close agreement between $\lambda^{\rm st}$ and $\lambda^{\rm var}$ ($\kappa_{\rm G} \approx 1$) was obtained for Ru-modified cyt c[22,64] and b_5,[64] multi-heme cytochromes STC,[24] NtrfB,[25] MtrF[65] and MtrC,[25] cytochrome c oxidase,[66] the blue Cu-protein azurin[23] as well as a porphyrine-binding four-helix bundle protein[64] (for the latter, $\kappa_{\rm G} \approx 3.7$ in our early study[67] reversed to $\kappa_{\rm G} \approx 1.1$ when protein and water were treated electronically polarizable[64]). Simulations were typically carried out on the 10-50 ns time scale which was sufficient to converge both reorganization free energies $\lambda^{\rm st}$ and $\lambda^{\rm var}$ arising from nanosecond or faster protein motions. However, it may well be that ergodicity-breaking protein motions occur at longer times that are closer to the time scale of ET in these proteins, typically microseconds. To test this possibility we calculate in the present work $\lambda^{\rm st}$ and $\lambda^{\rm var}$ for oxidation of native horse-heart cyt c from MD simulations run over hundreds of nanoseconds, an order of magnitude longer than in our previous works. Moreover, we investigate the sensitivity of results with regard to (i) the protein and water force field used (CHARMM vs AMBER), (ii) the inclusion of electronic polarizability for the redox active heme c cofactor using QM/MM calculations with the QM region treated at the level of density functional theory (DFT) or perturbed matrix method (PMM),[52,53,68–70] and (iii) the inclusion of electronic polarizability for protein and water using a polarizable force field with induced atomic dipoles. We choose cyt c because experimental reorganization free energies for oxidation in solution are well known and agree among different electrochemical measurements[71,72] and because simulation data from the group of Matyushov are available for comparison.[61–63]

Anticipating our results, we find no evidence for ergodicity-breaking effects in cyt c on the hundred nanosecond time scale, in contrast to Refs.[61–63] Both reorganization free energies

are about equal, $\lambda^{\mathrm{st}} \approx \lambda^{\mathrm{var}} \approx 1.0\,\mathrm{eV}$ without or with inclusion of electronic polarizability of the heme center, yet significantly overestimate experimental values obtained from electrochemistry, 0.58 eV.[71,72] Treating the protein and solvent electronically polarizable reduces both reorganization free energies by $\approx 40\%$ aligning the computed estimate with experiment. Variance reorganization free energies as large as the ones reported in Refs.[61–63] (close to 3 eV) are only obtained if the electrostatic field at the heme site is scaled by a factor of about 5. Hence, while ergodicity-breaking effects may occur for other biological ET reactions, our present simulations suggest that this is not the case in cyt c. In the remainder of this paper we present in detail our simulation results followed by some concluding remarks.

Computational Details

MD with non-polarizable force fields

We set up the simulation system as reported in Ref.[61,63] Starting from the NMR solution structure of reduced horse heart cytochrome c (pdb id 1GIW[73]), 116 crystal waters from the 1YCC[74] crystal structure were added to 1GIW after aligning the two PDB structures. One missing hydrogen in the first residue GLY was added to saturate the valence of a carbon atom (CA atom type). No counter ions were added as they were found to have a negligible effect on reorganization free energy (see Ref.[63]). This resulted in a total charge of $+7e/+8e$ for the reduced/oxidized protein. 33232 TIP3P water molecules were added to the simulation box giving a total of 101441 atoms. Simulations were carried out with two protein force fields, CHARMM27,[75] as in Ref.,[63] with the charges and bond parameters for the heme cofactor taken from Kaszuba *et al.*,[76] and with the AMBER03 protein force field[77] with heme atomic charges and bond parameters taken from previous simulations in our group.[25,64,78] The topologies for CHARMM27 and AMBER03 were generated with the psfgen tool in VMD[79] and LeaP in AMBER Tools 16,[77] respectively.

MD simulations were carried out with the SHAKE algorithm to constrain O-H bonds in

water molecules. Particle mesh Ewald was used for the electrostatics with a real space cutoff of 12 Å and the same cutoff was applied for Van-der-Waals interactions. The solvated protein in the reduced oxidation state was initially minimized for 5000 steps and subsequently equilibrated for 500 ps with all protein atoms kept frozen. The temperature was rescaled to 300 K every 5000 steps and a Langevin barostat was applied with a target pressure of 1 bar, piston period of 100 fs, and piston decay time of 50 fs. The protein was then slowly released by applying harmonic restraints around the crystallographic positions with decreasing force constants of 99, 25, 1.0, 0.1, and 0.001 kcal mol^{-1} Å^{-2}. For each restraining force 500 ps MD simulations in the NPT ensemble were carried out using a 1 fs MD time step. The thermostat damping coefficient was 1 ps^{-1} and the barostat parameters were the same as before. Then all restraints were removed and the protein equilibrated for 10 ns in the NPT ensemble, followed by equilibration of 10 ns in the NVT ensemble using a 2 fs time step. After equilibration, the size of the simulation box was 101.08 Å × 101.08 Å × 101.08 Å. Finally the temperature was decreased to 290K with a cooling rate of 1K/ns. A production run trajectory of 288.0 ns (250 ns) was generated in the NVT ensemble at $T = 290$K using the Langevin thermostat for CHARMM27 (AMBER03). Simulations of oxidized cytochrome c were initiated from an equilibrated snapshot of the reduced protein. The system was equilibrated for 20 ns in the NVT ensemble at 290 K, followed by a production run of 288.5 ns for CHARMM27 and 250 ns for AMBER03. Snapshots were saved with the frequency of 10 ps in the production runs. All classical MD simulations were done with the NAMD code.[80]

Energy gap from non-polarizable MM calculations. The energy gap Eq. 5 was calculated for 28,000 (25,000) equidistantly spaced snapshots sampled along each of the CHARMM27 (AMBER03) production trajectories in reduced and oxidized states (sampling frequency = 100 snapshots/ns), as well as for a sub-ensemble of 513 equidistantly spaced snapshots along each trajectory (sampling frequency = 2 snapshots/ns). Reorganization free energies obtained with the lower sampling frequency reproduced the values obtained with the higher sampling frequency to within 0.05 eV.

Energy gap from QM(DFT)/MM calculations. QM(DFT)/MM calculations of the energy gap Eq. 5 were carried out on the above 513 equidistantly spaced snapshots taken from each of the classical MD simulations in reduced and oxidized states to probe the effect of polarizability of the QM region on reorganization free energy. Two different QM models in QM(DFT)/MM calculations were employed for the CHARMM27 trajectories (models 1 and 2) and only one QM/MM model for AMBER03 trajectories (model 1). Model 1 comprises of the heme ring, axial ligands and side chains excluding the propionates (Figure 2B). The latter were saturated with hydrogen atoms at the positions CAA-CBA and CAD-CBD to CAA-H and CAD-H, respectively. The CB-CA bonds of the cysteine linkages, axial histidine and methionine were cut and saturated with a hydrogen atom to CB-H. A small amount of charge was redistributed from Fe to the -CH_2-COO propionate side chains in the MM region to enforce an integer total charge of the QM region. In model 2 (Figure 2C), used in Ref.,[61–63] the two propionates where included in their deprotonated form. The bonds of the axial ligands HIS18 and MET80 and of cysteine linkage CYS14 were capped at the backbone C-N position and saturated to C-H. The total charge of the QM region is $0/+1e$ for reduced/oxidized state in model 1 and $-2e/-1e$ in model 2. QM model 2 is not an ideal set-up for QM/MM calculations because the propionates form a salt bridge with neighbouring positively charged residues and both should be either included or excluded from the QM region rather than treated at separate levels of theory. Moreover, the polar amide bonds of the amino acid residues are cut and saturated with hydrogens, instead of the apolar carbon-carbon bonds as is best practice. QM model 1 was designed to remove these issues. However, the reorganization free energies were not very sensitive to these different set-ups (see Table 1). In both models, the charge distribution for the (non-polarizable) MM atoms was the same for reduced and oxidized states. The QM/MM energy gaps were calculated with the CP2K package.[81] The QM region was described at DFT level with PBE[82] functional, DZVP basis set and GTH atomic pseudopotentials.[83] The spin multiplicities for the reduced and oxidized states were singlet and doublet, respectively. For each snapshot, the

QM part was centered in a 30Å × 30Å × 30Å box which guaranteed at least 7.0 Å vacuum padding in each direction. The generalized hybrid orbital method[84] was used to link QM and MM atoms at their boundary. The MM settings were the same as used in the classical MD simulations above. The wavefunction gradient was converged to 10^{-5} a.u.

Energy gap from QM(PMM)/MM calculations. QM(PMM)/MM calculations of the energy gap Eq. 5 with potential energies from Eq. 8-9 were carried out on the 28,000 equidistantly spaced snapshots sampled along each of the CHARMM27 production trajectories and the sub-ensemble of 513 snapshots as described previously. For evaluation of the energy gap along the reduced trajectory, the unperturbed ground and excitation energies $\epsilon_i^{(M)}$ and the transition-dipole-moment matrix elements $\boldsymbol{\mu}_{ij}^{(M)}$ were calculated for reduced (M = R) and oxidized (M = O) QM model 2 on the reduced crystal structure geometry using ZINDO/S semi-empirical electronic structure calculations, as implemented in Gaussian 16.[85] These parameters remained unchanged for all the snapshots. For evaluation of the energy gap along the oxidized trajectory, similar calculations for $\epsilon_i^{(M)}$ and $\boldsymbol{\mu}_{ij}^{(M)}$ were carried out on the oxidized crystal structure geometry. The electrostatic potential and field on the Fe atom, V_{Fe} and $\mathbf{E}_{\mathrm{Fe}}$, were obtained from force field calculations within periodic boundary condition using NAMD.[80]

Energy gap from polarizable MM calculations. The energy gap Eq. 5 was also calculated with the polarizable AMBER02 force field[77] and POL3 water model[77] on the same 513 snapshots for which QM(DFT)/MM calculations were carried out (i.e. on configurations obtained from MD with AMBER03 force field[77] and TIP3P water). Electronic polarizability of the MM atoms is modelled by atomic and isotropic induced dipoles, while the polarizability of the atoms treated as QM atoms in QM/MM calculations (QM model 1) were set to zero. This choice was made to probe the effect of the polarizability of the MM region (outer-sphere) only. The induced dipoles were iterated until successive estimates agreed to within 10^{-4} debye in the root mean square sense. All calculations with polarizable force fields including the MD simulations below were carried out with the sander program in AMBER

Tools 16.[77]

MD with electronically polarizable force field

For the MD simulation with explicitly polarizable force fields, the initial structure for the oxidized state was extracted from a snapshot of the previous AMBER03 production run trajectory in the oxidized state. Due to increased computational cost in the Ewald summation in the polarizable MD, the system size was reduced by decreasing the number of water molecules to 6544. We checked the convergence of reorganization free energy with size of the solvation shell at the non-polarizable MD level and find that this system size is sufficient. The system with reduced number of water molecules was initially equilibrated for 10 ns in the NPT ensemble with the non-polarizable AMBER03 force field and TIP3P water and then equilibrated with the polarizable AMBER02 force field and POL3 water: 500 ps in the NVT ensemble, 2.5 ns in the NPT ensemble to 290 K and 1.013 bar using a Langevin barostat with piston period 100 fs, piston decay time and thermostat damping coefficient 15.0 ps^{-1}, and finally 5 ns in the NVT ensemble at a fixed cell size of 59.5Å $\times$ 59.4Å $\times$ 59.4Å. Instead of solving the induced dipoles iteratively at each step, we adopted the Car-Parinello scheme for efficient MD propagation, wherein each dipole was assigned a fictitious mass of 0.33 a.u. Production runs were carried out for 50 ns with a MD time step of 1 fs. Polarizable MD simulation of the reduced protein was carried out similarly with a starting structure extracted from a snapshot of the previous AMBER03 production run trajectory in the reduced state.

Energy gap from polarizable MM calculations. The energy gap Eq. 5 was calculated with the polarizable AMBER02 force field[77] and POL3 water model[86] on 10 ps equidistantly spaced snapshots taken from each of the 50 ns MD trajectories run for reduced and oxidized states with the AMBER02 force field[77] and POL3 water. The induced dipoles were iterated until successive estimates agreed to within 10^{-4} debye in the root mean square sense.

Results and Discussion

Reorganization free energies from vertical energy gaps

The Stokes and variance reorganization free energies, λ^{st} and λ_M^{var} respectively, are defined by

$$\lambda^{\mathrm{st}} = (\langle \Delta E \rangle_{\mathrm{R}} - \langle \Delta E \rangle_{\mathrm{O}})/2 \tag{3}$$

$$\lambda_M^{\mathrm{var}} = \frac{\sigma_M^2}{2k_{\mathrm{B}}T}, \quad M = \mathrm{R},\, \mathrm{O}, \tag{4}$$

where ΔE is the vertical energy gap,

$$\Delta E(\mathbf{R}^N) = E_{\mathrm{O}}(\mathbf{R}^N) - E_{\mathrm{R}}(\mathbf{R}^N), \tag{5}$$

$E_M(\mathbf{R}^N)$ the potential energy of oxidized ($M = \mathrm{O}$) and reduced cyt c ($M = \mathrm{R}$) at the nuclear configuration $\mathbf{R}^N$, $\langle \cdots \rangle_M$ denotes the thermal average on the potential energy surface of redox state M, and

$$\sigma_M^2 = \langle (\Delta E - \langle \Delta E \rangle_M)^2 \rangle_M \tag{6}$$

is the variance of the vertical energy gap fluctuations. In the limit of linear response (i.e., Gaussian gap fluctuations) and ergodic sampling, $\lambda^{\mathrm{st}} = \lambda_{\mathrm{R}}^{\mathrm{var}} = \lambda_{\mathrm{O}}^{\mathrm{var}}$.[23] The thermal averages are obtained by sampling the energy gap ΔE along MD trajectories for oxidized and reduced solvated cytc. We set up the same simulation system as in Refs.[61–63] to ensure a fair comparison, see Figure 2 for a snapshot of the solvated protein. We then investigated the sensitivity of the computed energy gaps and reorganization free energies on (i) the force field used for MD simulation, CHARMM27[75] versus AMBER03[77] (both non-polarizable) (ii) the inclusion of electronic polarizability for the heme cofactor ("inner-sphere") via QM(DFT)/MM[81] and QM(PMM)/MM[85] calculations and (iii) the inclusion of electronic polarizability for the protein and water ("outer sphere") using the electronically polarizable AMBER02 protein force field[77] and POL3 water[86] where isotropic atomic dipoles are self-consistently relaxed. Sim-

ulation protocols and details on the energy gap calculations can be found in *Computational Details.* The numerical results are summarized in Table 1.

Force fields: CHARMM27 vs AMBER03

The vertical energy gaps along trajectories for reduced and oxidized cyt c are shown in Figure 3A (CHARMM27) and Figure 3B (AMBER03). They fluctuate relatively stably around their mean values on the simulated time scale of $\approx 250\,\mathrm{ns}$, and the distribution of gap energies fit Gaussian functions almost perfectly (R^2 >0.999) for both force fields. The convergence of reorganization free energies λ^{st} (Eq. 3) and λ^{var} (Eq. 4) with respect to simulation time is shown in Figure 3C and Figure 3D. While λ^{st} is converged after a few ns, it takes significantly longer (50 ns for CHARMM27, 150 ns for AMBER03) to obtain values for λ^{var} that are close to the final result. This is not surprising as it is well known that mean square fluctuations take longer to converge than the mean. The somewhat abrupt changes in the accumulated average of λ^{var} for AMBER03 are related to short drifts in the energy gap due to rare protein fluctuations. The RMSD with respect to the crystal structure was stable and reasonably small for AMBER03 trajectories, averaging to about 2.0 Å in reduced and oxidized states.

The two force fields give almost identical values for λ^{st} to within the statistical error bar, 0.95 and 0.93 eV for CHARMM27 and AMBER03, respectively. For CHARMM27 this value is almost perfectly matched by $\lambda_{\mathrm{R}}^{\mathrm{var}}$ and $\lambda_{\mathrm{O}}^{\mathrm{var}}$, 0.96 eV for both oxidation states. For AMBER03 the two variance reorganization free energies differ by 0.2 eV but this difference is equal to the statistical error bar for $\lambda_{\mathrm{O}}^{\mathrm{var}}$ implying that present simulations on the 100 ns timescale are still insufficient to fully converge the fluctuations of the energy gap for this force field. However, the average $\lambda^{\mathrm{var}} = (\lambda_{\mathrm{R}}^{\mathrm{var}} + \lambda_{\mathrm{O}}^{\mathrm{var}})/2 = 0.93\,\mathrm{eV}$ matches perfectly λ^{st}. Disregarding this issue, we conclude that for both force fields the ratio $\kappa_{\mathrm{G}} = \lambda^{\mathrm{var}}/\lambda^{\mathrm{st}} = 1.0$ as in Marcus theory and that there is no signature of non-ergodic effects at the level of non-polarizable force field simulations on the time scale of a few 100 ns. This result and the

numerical values for reorganization free energy are similar to the ones reported by Matyushov and co-workers for the CHARMM27 force field.[61]

Electronic polarizability of heme

QM(DFT)/MM calculations of the energy gap Eq. 5 were carried out on structures sampled from the above classical MD calculations. Two QM models were used, model 1 comprised of heme ring and axial ligands (Figure 2B), and model 2 which included, in addition, the propionates (Figure 2C). The latter model was used in Ref.[61–63] For each structure the electronic potential energies for oxidized and reduced states, E_{O} and E_{R} in Eq. 5, are obtained by self-consistent iteration of the Kohn-Sham equations for the QM region in the electrostatic field generated by the fixed point charges of the MM region applying periodic boundary conditions. The potential energies are comprised of the QM, QM/MM and MM interaction energy,

$$E_M = E_M^{\mathrm{QM}} + E_M^{\mathrm{QM/MM}} + E_M^{\mathrm{MM}}; \quad M = \mathrm{O},\, \mathrm{R} \tag{7}$$

where E_M^{MM} is independent on the oxidation state, hence does not contribute to the energy gap. To reduce the computational effort, we first determined at the MM level the largest equidistant spacing, or equivalently, the minimum sampling frequency of snapshots along the ≈ 250 ns MD trajectories that reproduced the reorganization free energies obtained for the originally chosen sampling frequency (100 snapshots/ns) to within 0.05 eV. We obtain a minimum sampling frequency of 2 snapshots/ns for both force fields (see Figure 3E,Figure 3F), which corresponds to 513 snapshots along the ≈ 250 ns MD trajectories. QM(DFT)/MM energy gap calculations were carried out on this sub-ensemble of configurations.

The accumulated average of the reorganization free energies at the QM(DFT)/MM level is shown in Figure 4A (CHARMM27 trajectories) and B (AMBER03 trajectories). We find that the values are very similar to the ones from classical MD calculations. λ^{st} slightly decreases and λ^{var} slightly increases, but the difference between the two reorganization free

energies remains within two (CHARMM27) and one (AMBER03) errorbars, giving $\kappa_{\rm G}=1.14$ (QM model 1, CHARMM27 trj) and 1.20 (QM model 2, CHARMM27 trj) and 1.07 (QM model 1, AMBER03 trj). Hence, we do not observe a truly significant increase in the variance reorganization free energies upon inclusion of heme electronic polarizability at the DFT level of theory. This is in line with simulation data from Ref.[69] ($\kappa_{\rm G}=1.26$), but in contrast to the results of Ref.,[63] where $\kappa_{\rm G}$ values as large as 2.3 were reported. In the latter two studies electronic polarizability of the QM region was included by the perturbed matrix method (PMM), which differs in some important aspects from the QM(DFT)/MM method as we explain in the following.

QM(PMM)/MM. In the perturbed matrix method (PMM)[52,53,68–70] electronic structure calculations are carried out for the QM center in vacuum and the interaction with the electrostatic field generated by the MM atoms is calculated perturbatively via a multipole expansion of the QM center, usually truncated at second order,

$$H_{ij}^{(M)} = (\epsilon_i^{(M)} + Q_{\rm Fe}^{(M)} V_{\rm Fe})\delta_{ij} - \boldsymbol{\mu}_{ij}^{(M)} \cdot \boldsymbol{E}_{\rm Fe} \tag{8}$$

$$E_M = {\rm Min}[\{{\rm EV}_i(\mathbb{H}^{(M)})\}], \quad M = {\rm R},\, {\rm O}, \tag{9}$$

where $\mathbb{H}^{(M)}$ is the perturbed Hamiltonian matrix for oxidation state M with matrix elements $H_{ij}^{(M)}$, $\epsilon_i^{(M)}$ are the unperturbed ground and excited electronic state energies of the isolated cofactor, $Q_{\rm Fe}^{(M)}$ is the total charge of the QM region in redox state M assumed to be located on the Fe atom (i.e., $Q_{\rm Fe}^{({\rm O})}=-1e$, $Q_{\rm Fe}^{({\rm R})}=-2e$), $V_{\rm Fe}$ is the Coulomb potential and $\boldsymbol{E}_{\rm Fe}=-\nabla V|_{\rm Fe}$ the corresponding electric field on the Fe atom due to the MM atoms, and $\boldsymbol{\mu}_{ij}^{(M)}=-e\langle\phi_i|\boldsymbol{r}|\phi_j\rangle$ are the transition-dipole-moment matrix elements obtained from QM calculations in gas phase. The potential energy of redox state M, E_M in Eq. 9, is the lowest eigenvalue (EV) of $\mathbb{H}^{(M)}$ and used for the calculation of the energy gap Eq. 5. Following the protocol of Ref.[61,63] we use ZINDO/S semi-empirical electronic structure calculations[85] on QM model 2 of the heme cofactor to obtain $\epsilon_i^{(M)}$ and $\boldsymbol{\mu}_{ij}^{(M)}$. $V_{\rm Fe}$ and $\boldsymbol{E}_{\rm Fe}$ for protein and solvent configurations

are obtained from the CHARMM27 trajectory. We note that ZINDO/S is not expected to be the most reliable method for the calculation of transition dipoles, and potentially better DFT-based approaches are available for large molecules. However, our goal here is to reproduce the results of Ref.[61,63] which is why we use ZINDO/S in present calculations.

The reorganization free energies obtained from QM(PMM)/MM are shown in Figure 4 A. We find that the energy gap distributions are again well described by Gaussians in agreement with previous QM(PMM)/MM calculations of horse-heart cyt c.[53] Both λ^{st} and λ^{var} match very well the values obtained from present MM and QM(DFT)/MM calculations; we obtain $\kappa_{\mathrm{G}} = 1.20$ (QM model 2, CHARMM27 trj) which is virtually identical with the result from QM(DFT)/MM calculations. A large increase in λ^{var} as reported in Ref.[63] is not observed even though the same system set-up is now used. We do obtain similarly large electronic polarizabilities for the heme cofactor as in Ref.[61,63] (54 Å^3 and 27 Å^3 for the reduced and oxidized states when including 100 electronic states for construction of $\mathbb{H}^{(M)}$), but they do not lead to a significant enhancement of the energy gap fluctuations. The reason is that the electrostatic field at the Fe site is relatively modest (0.05-0.5 V/Å) in our simulations so that the off-diagonal terms $\boldsymbol{\mu}_{ij}^{(M)} \cdot \boldsymbol{E}_{\mathrm{Fe}}$ in Eq. 8 are small compared to the diagonal energy differences $\epsilon_i^{(M)} - \epsilon_j^{(M)}$ resulting in little mixing between the states. Indeed, if polarizability is entirely neglected and the second term in Eq. 8 is set to zero, λ^{var} decreases by no more than 0.05 eV. To obtain values for λ^{var} as large as the ones reported in Ref.[61,63] (2-3 eV), the electrostatic field due to protein and water would need to be scaled by a factor of about 5 in our simulations. We also note that while the heme polarizability converges very slowly with the number of electronic states used to construct $\mathbb{H}^{(M)}$ (see Table S1), λ^{var} is converged after including only the ten lowest states (Table S2). This gives credence to the QM(PMM)/MM calculations of Ref.[69] where 13 states were included. The energy gap auto-correlation function shows the typical signatures for solvated redox proteins (Figure S1), a sharp initial decay on the 100 ps time scale due to relaxation of bulk solvent and amino acid side chains, and a longer decay to zero on the 10 ns time scale characteristic of the slower

backbone motions. The calculated correlation time is around 60 ns.

Electronic polarizability of protein and water

Finally, we investigate the effect of electronic polarizability of the MM region (protein and water) on reorganization free energies. To this end, the energy gap Eq. 5 is calculated with the polarizable AMBER02 force field[77] and POL3 water[86] on the same set of structures for which QM(DFT)/MM calculations were carried out (i.e. AMBER03 + TIP3P water trajectories). Electronic polarizability of the MM atoms is modelled by atomic and isotropic induced dipoles, while the polarizability for the atoms of the QM region was set to zero. This choice was made to probe the effect of the polarizability of the MM region (outer-sphere) only. The results are shown in Figure 4C. We find that reorganization free energies now decrease dramatically from 0.93 eV for non-polarizable MM calculations to $\lambda^{\mathrm{st}} = 0.69$ and $\lambda^{\mathrm{var}} = 0.55\,\mathrm{eV}$. These values are in good agreement with the experimental estimate from electrochemistry, 0.58 eV.[71]

In previous work on electron self-exchange between Ru-aqua ions a similar reduction in reorganization free energy was obtained upon treating the solvent electronically polarizable, but this reduction was partly offset when both MD and energy gap calculations were consistently carried out with the same polarizable force field due to differences in the solvation structure between non-polarizable and polarizable water models.[87] By contrast, no such partial cancellation is observed here for solvated cyt c when both polarizable MD simulations and energy gap calculations are carried out with the AMBER02 force field and POL3 water. On the contrary, the reorganization free energies decreased slightly further to $\lambda^{\mathrm{st}} = 0.53\,\mathrm{eV}$ and $\lambda^{\mathrm{var}} = 0.46\,\mathrm{eV}$, corresponding to a decrease of 43% and 50% compared to the values from non-polarizable MM calculations. If the inner-sphere contribution of the heme cofactor, here described at the MM level, is replaced by a QM description ($\lambda_{\mathrm{i}} = 0.025\,\mathrm{eV}$ for isolated heme c cofactor in vacuum[22]), the final result is very close to experiment, $\lambda^{\mathrm{st}} = 0.56\,\mathrm{eV}$ and $\lambda^{\mathrm{var}} = 0.49\,\mathrm{eV}$, while κ_{G} remains close to unity.

The reduction in reorganization free energy upon inclusion of electronic polarizability of the outer sphere is in line with a bulk of existing simulation data for electron transfer and oxidation reactions in proteins[22,23,25,64–66] and aqueous transition metal ions.[87–91] We have shown that MD reorganization free energies in Ru-modified proteins are strongly overestimated compared to the experimental values by Gray and Winkler if electronic polarizability of protein and water is not explicitly accounted for but in much better agreement if included.[23,64,66,87] Along the same lines, the reorganization free energies for oxidation of simple transition metal ions in liquid water, such as aqueous $Ru(bpy)_3^{2+}$[88] and Mn^{2+},[90] were obtained in excellent agreement with experimental values from liquid jet photo-emission spectroscopy by Winter and co-workers[88,90] when the same polarizable POL3 water was used as in present protein simulations.

The importance of outer-sphere electronic polarizability may be explained by continuum theory, which predicts that outer-sphere reorganization free energy is proportional to the inverse of Pekar factor, $1/(1/\epsilon_{\rm op} - 1/\epsilon_{\rm s})$. For aqueous cyt c, the optical dielectric constant $\epsilon_{\rm op}$ may be estimated from experimental data to be 1.84[22] while for non-polarizable force fields $\epsilon_{\rm op} = 1$. Hence, assuming $\epsilon_{\rm s} >> \epsilon_{\rm op}$ (which should be fulfilled for solvated proteins), the reorganization free energy is predicted to be overestimated by a factor $\approx 1/1.84$ or 46% if protein and water are not treated electronically polarizable. This agrees very well with present simulation results, even though for other proteins we typically found a somewhat smaller effect of 30-40%.[23]

On the contrary, it was suggested some time ago that the Pekar factor gives a much too strong dependence of reorganization free energy on the optical dielectric[92] and recently it was shown for some model systems that reorganization free energy is nearly insensitive or even increases with increasing optical dielectric constant.[93] While we are cautious to generalize results from simple model systems to complex proteins, we note that switching from a non-polarizable to a polarizable force field is not equivalent to simply changing the optical dielectric constant of the medium. When electronic polarizability is introduced in

the force field, the point charges are scaled back from their effective (larger) values in the condensed phase to the smaller values in the gas phase. As our simulations suggest, in the case of cyt c the reduction in reorganization free energy due to the smaller point charges is not compensated for by the induced dipoles and/or additional structural relaxation in response to the introduction of induced dipoles, resulting in a significant net reduction in reorganization free energy.

Conclusions

With increasing computational capabilities over the last decades it has become possible to push the accessible time scale of protein simulations from picoseconds[94] to microseconds and beyond. In the context of redox protein simulation, this has allowed us to calculate the parameters determining the ET kinetics, e.g. energy gap fluctuations, over much longer time scales, for some systems approaching the actual time scale of the thermal ET reaction, microseconds in case of cyt c. This has subsequently led to numerical evidence for Matyushov's hypothesis that in certain redox proteins (in particular, cyt c and plastocyanin) ET occurs on the physiological time scale because of ergodicity-breaking effects in the energy gap fluctuations and that ET would be too slow otherwise.

In this work we have thoroughly investigated this claim for oxidation of aqueous cytochrome c and have not found evidence for ergodicity breaking on the 250 ns time scale. Similar values for Stokes and variance reorganization free energies are obtained, $\lambda^{\mathrm{r}} \approx \lambda^{\mathrm{st}} \approx \lambda^{\mathrm{var}}$, with a variety of state-of-the-art methodologies ranging from non-polarizable MD simulations, QM/MM calculations with polarizable QM center at DFT and PMM level and polarizable MD simulation. Our results indicate that ET in solvated cyt c is an ergodic process and well described by linear response, i.e., Gaussian solvation theory; in other words, cyt c is a classic Marcus system. According to our simulations the overestimation of experimental reorganization free energies for cyt c typically obtained with non-polarizable force fields

is due to the missing electronic polarizability of the protein and water, in contrast to the ergodicity-breaking hypothesis advocated by Matyushov and co-workers.

Ergodicity-breaking is certainly an interesting and conceivable hypothesis for accelerating biological ET without sacrificing driving force and it may well apply to other redox proteins. Reviewing our previous simulation results, there are some proteins where reorganization free energies are somewhat overestimated when compared to experimental data even when the AMBER02 polarizable force field and POL3 water was used in the calculations.[23,64] Yet, Stokes and variance reorganization free energy sampled over 10-50 ns were still very similar implying that non-ergodic effects were not present on that (relatively short) time scale.[64] Possible reasons for the remaining overestimation in calculated reorganization free energy could be deficiencies in the polarizable force field model used (POL3 is known to underestimate electronic polarization effects[95]) or, indeed, the occurrence of ergodicity-breaking effects on longer time scales. Finding strong numerical evidence for ergodicity-breaking effects in thermal biological ET will require very carefully conducted MD simulations on long (microsecond) time scales with accurate electronically polarizable force fields. This presents a formidable challenge to contemporary biomolecular simulations.

Supporting Information. Convergence of electronic polarizability and reorganization free energy with number of excited states used in QM(PMM)/MM calculations, gap-energy autocorrelation functions (ACFs) and their time integrals.

Acknowledgement

X.J. was supported by a Ph.D. studentship cosponsored by the Chinese Scholarship Council and University College London. Z.F. was supported by EPSRC Grant No. EP/M001946/1. Via our membership of the UK's HEC Materials Chemistry Consortium, which is funded by EPSRC (EP/L000202, EP/R029431), this work used the ARCHER UK National Supercomputing Service (http://www.archer.ac.uk). We are grateful to the UK Materials and

Molecular Modelling Hub for computational resources, which is partially funded by EPSRC (EP/P020194/1). The authors acknowledge the use of the UCL Grace High Performance Computing Facility (Grace@UCL), and associated support services, in the completion of this work.

Table 1: Computed reorganization free energies for oxidation of solvated horse-heart cytochrome c (all values in eV).[a]

CHARMM ff

	MM(np)[e]		QM(DFT)/MM(np)[h]		QM(PMM)/MM(np)			
	SF1[f]	SF2[g]	QM1[i]/SF2[g]	QM2[j]/SF2[g]	QM2[k,j]/SF1[f]	QM2[k,j]/SF2[g]	Ref[69][l]	Ref[63][k,j]
$\lambda^{\mathrm{st}\,b}$	0.95 ± 0.01	0.95 ± 0.01	0.89 ± 0.01	0.86 ± 0.01	1.00 ± 0.01	1.00 ± 0.01	0.89	1.32
$\lambda_{\mathrm{R}}^{\mathrm{var}\,c}$	0.92 ± 0.06	0.96 ± 0.08	1.00 ± 0.08	1.03 ± 0.09	1.23 ± 0.08	1.12 ± 0.08	1.32	2.97
$\lambda_{\mathrm{O}}^{\mathrm{var}\,c}$	0.92 ± 0.03	0.96 ± 0.06	1.03 ± 0.06	1.03 ± 0.08	1.24 ± 0.07	1.31 ± 0.12	0.92	2.97
κ_{G}^{d}	0.97	1.01	1.14	1.20	1.23	1.20	1.26	2.25

AMBER ff

	MM(np)[e]		QM(DFT)/MM(np)[h]	MM(pol/np)[m]	MM(pol/pol)[n]
	SF1[f]	SF2[g]	QM1[i]/SF2[g]	SF2[g]	SF1[f]
$\lambda^{\mathrm{st}\,b}$	0.92 ± 0.01	0.93 ± 0.01	0.89 ± 0.01	0.69 ± 0.01	0.53 ± 0.01
$\lambda_{\mathrm{R}}^{\mathrm{var}\,c}$	0.80 ± 0.04	0.80 ± 0.05	0.92 ± 0.06	0.46 ± 0.03	0.39 ± 0.03
$\lambda_{\mathrm{O}}^{\mathrm{var}\,c}$	1.02 ± 0.16	1.06 ± 0.17	0.98 ± 0.13	0.63 ± 0.10	0.52 ± 0.04
κ_{G}^{d}	0.99	1.00	1.07	0.79	0.86

[a] The experimental reorganization free energy is 0.58 eV.[71] The statistical uncertainties of mean and variance of the computed energy gap Eq. 5 are estimated by the uniformly minimum variance unbiased estimator,[96] $u(\langle \Delta E \rangle) = \sigma/\sqrt{n/s}$, $u(\delta \Delta E^2) = \sigma^2 \sqrt{2/(n/s-1)}$, where n is the number of data points, σ is the standard deviation and s the statistical inefficiency. The statistical uncertainties for the reorganization free energies are estimated by Gaussian error propagation.

[b] Stokes reorganization free energy Eq. 3.

[c] Variance reorganization free energies Eq. 4.

[d] $\kappa_{\mathrm{G}} = (\lambda_{\mathrm{R}}^{\mathrm{var}} + \lambda_{\mathrm{O}}^{\mathrm{var}})/(2\lambda^{\mathrm{st}})$.

[e] Energy gap and MD calculations with electronically non-polarizable (np) force fields, CHARMM27 or AMBER03 and TIP3P water, respectively. Reorganization free energy is the sum of inner and outer-sphere contributions, both computed at the MM level of theory. The MM inner-sphere contribution 0.022 eV is in good agreement with DFT(PBE) value 0.025 eV for a cofactor model in the gas phase.[22]

[f] Sampling frequency (SF) for energy gap calculation = 100 snapshots/ns.

[g] SF for energy gap calculation: 2 snapshots/ns.

[h] QM(PBE)/MM calculations on trajectories sampled with CHARMM27 or AMBER03 and TIP3P water, respectively.

[i] See Figure 2B and *Computational Details* for a description of QM model 1.

[j] See Figure 2C and *Computational Details* for a description of QM model 2.

[k] QM(PMM)/MM calculations on trajectories sampled with CHARMM27 and TIP3P water at $T = 290$K, respectively.

[l] QM(PMM)/MM calculation for yeast cytochrome c using trajectories sampled with gromos96 and SPC water at $T = 300$K, respectively. Numerical values were taken as reported in Ref.[61] For horse-heart cytochrome c a value of $\lambda^{\mathrm{st}} = 0.89$ eV was reported in Ref.,[53] but no values for variance reorganization free energy.

[m] Energy gap calculation with electronically polarizable AMBER02 force field and POL3 water on trajectories sampled with non-polarizable AMBER03 force field and TIP3P water, respectively.

[n] Electronically polarizable AMBER02 / POL3 force-field MD and ΔE calculations.

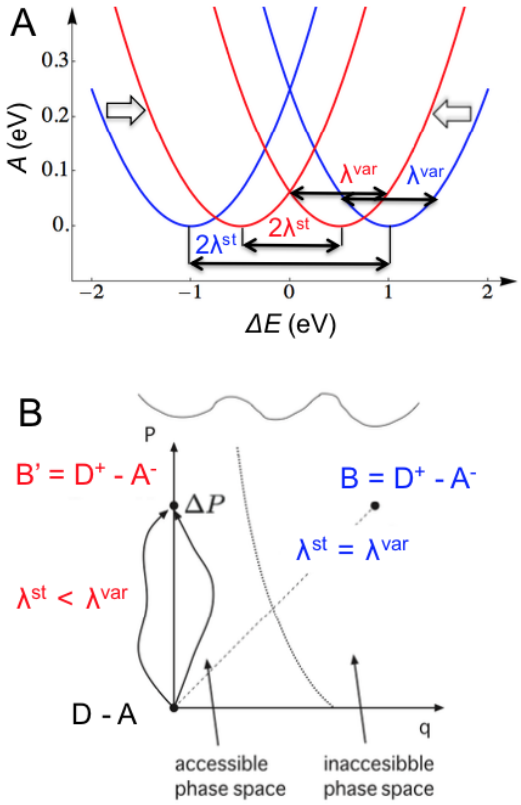

Figure 1: (A) Parabolic free energy profiles for ET in Marcus theory ($\lambda^{\mathrm{st}} = \lambda^{\mathrm{var}}$, blue) and when ergodicity is broken ($\lambda^{\mathrm{st}} < \lambda^{\mathrm{var}}$, red). In the latter case the protein conformational transition between the equilibrium configurations in reduced and oxidized states is too slow to occur on the ET time scale leading to a reduced Stokes shift as indicated by the block arrows. Consequently, the ET activation free energy is reduced by a factor $\kappa_{\mathrm{G}}^{-2} = (\lambda^{\mathrm{st}}/\lambda^{\mathrm{var}})^2$. (B) ET coupled to slow conformational change of the protein. The initial state is denoted D-A and the final state D^+-A^-. The reaction is described by a fast collective coordinate P for the protein and solvent modes coupling to ET and a coordinate q for the slow conformational change. ET along P occurs on a faster time scale than protein conformational change along q, resulting in the formation of a local minimum B' rather than the equilibrium state B on the product surface. Adapted with permission from Ref.[16] Copyright 2013, AIP Publishing LLC.

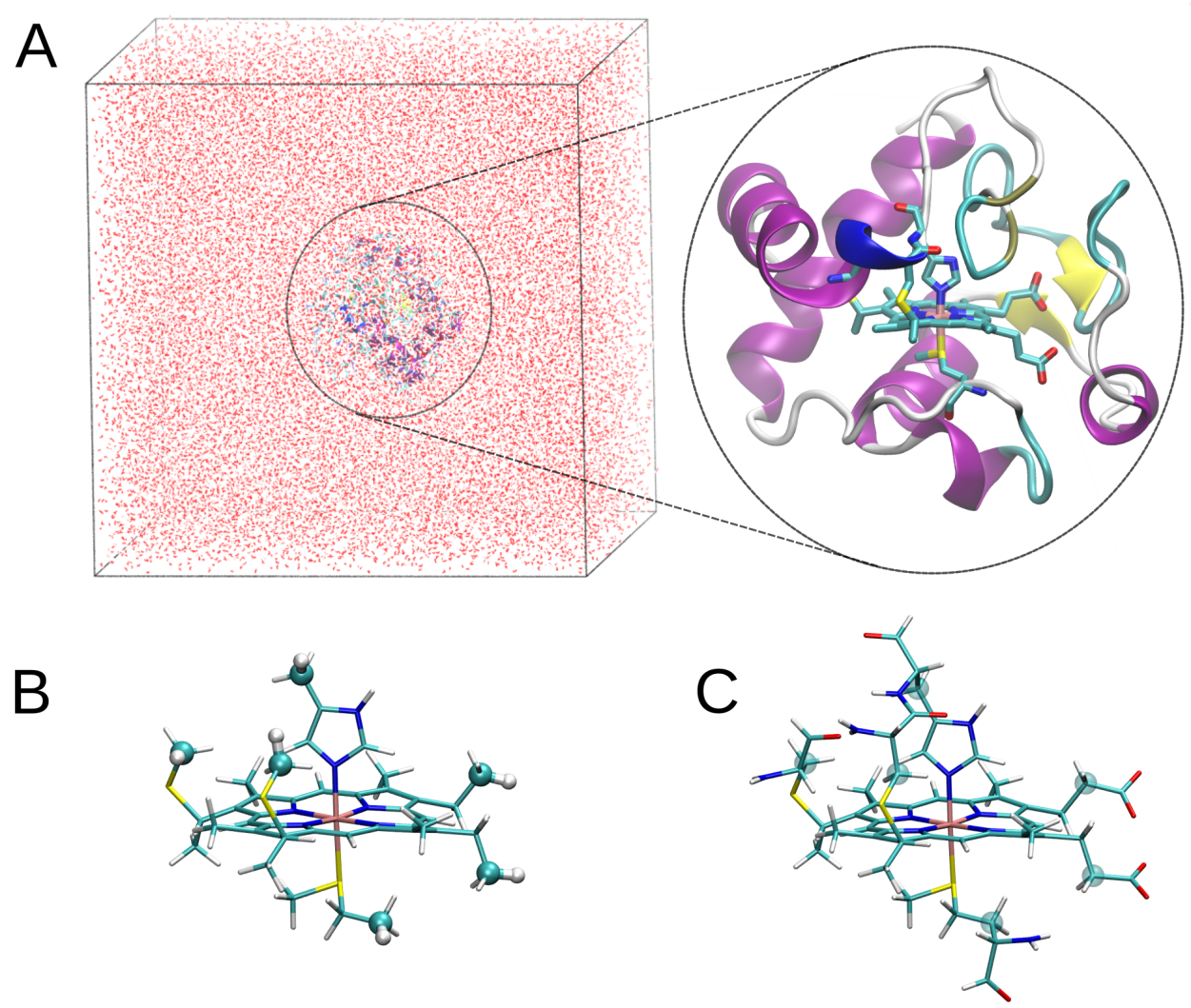

Figure 2: (A) Snapshot of the simulation box containing cytochrome c in aqueous solution (101441 atoms in total, 1745 protein atoms) and a zoom-in on the protein with the heme cofactor shown in stick representation (Fe, pink; S, yellow; O, red; N, blue; C, cyan) and secondary structure elements in cartoon representation. (B) QM model 1 and (C) QM model 2 in QM/MM calculations. In model 1, the two cysteine linkages and the two axial ligands were capped at the α-C and β-C bond and saturated with hydrogens (cyan and white spheres, respectively); heme propionates were not included in the QM region. In model 2, deprotonated propionates were included and the peptide bond was capped and saturated with hydrogens. The carbon atoms that were saturated with hydrogens in panel (C) are shown as cyan shaded spheres, for comparison. Model 2 was used in Ref.[63]

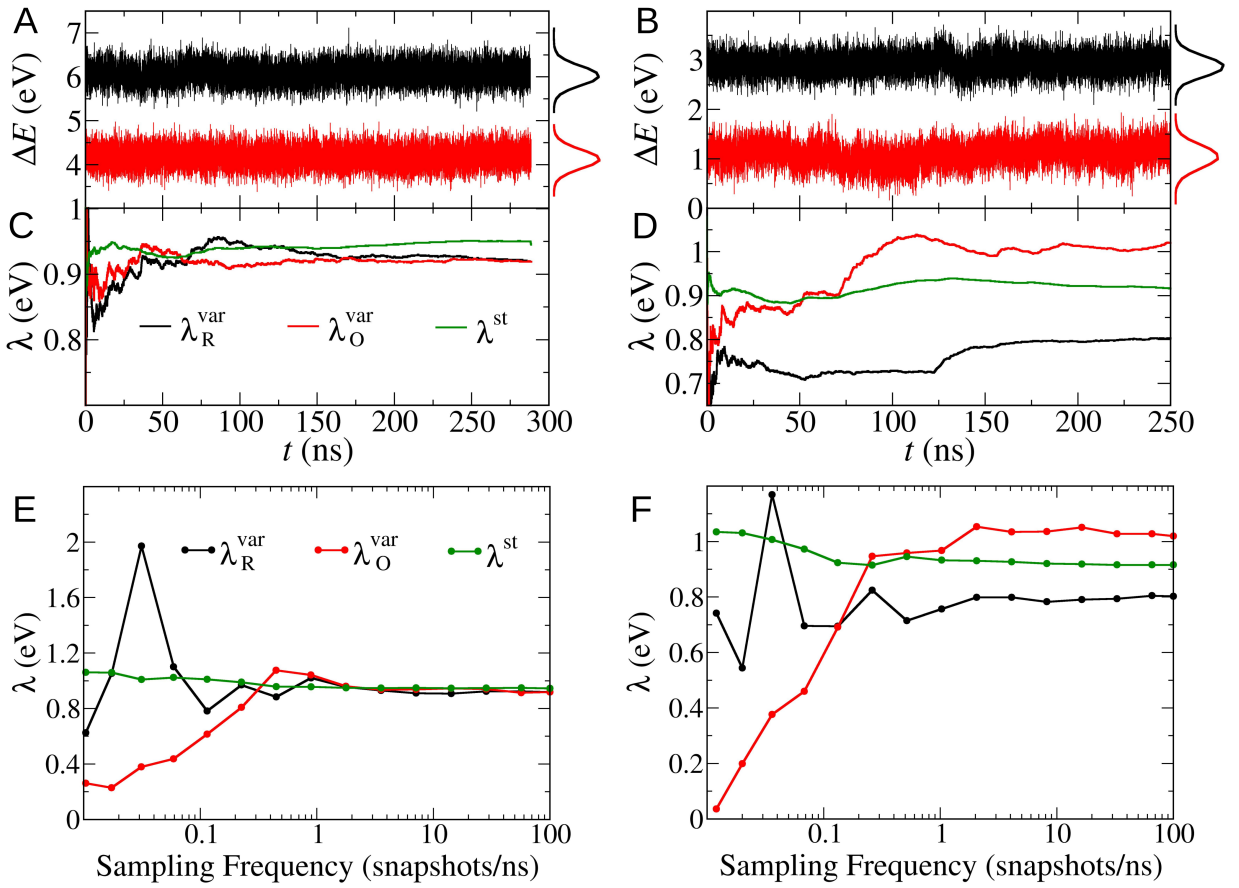

Figure 3: Fluctuations and convergence of the vertical energy gap ΔE (Eq. 5) for oxidation of solvated cytochrome c. MD trajectories are run with the non-polarizable (np) CHARMM27 ((A), (C), (E)) and AMBER03 force fields ((B), (D), (F)). In (A), (B) the fluctuations and distributions are shown for MD trajectories in the reduced (black) and oxidized (red) state. They are used for the calculation of the accumulated averages of Stokes and variance reorganization free energies, λ^{st} (Eq. 3), $\lambda_{\mathrm{R}}^{\mathrm{var}}$, $\lambda_{\mathrm{O}}^{\mathrm{var}}$ (Eq. 4), respectively (panels (C), (D)). The convergence of the reorganization free energies with respect to the sampling frequency (SF) of snapshots at constant trajectory length ($\approx$ 250-300 ns) is shown in panels (E) and (F). Convergence to within 0.05 eV is reached at 2 snapshots/ns (SF2 in Table 1).

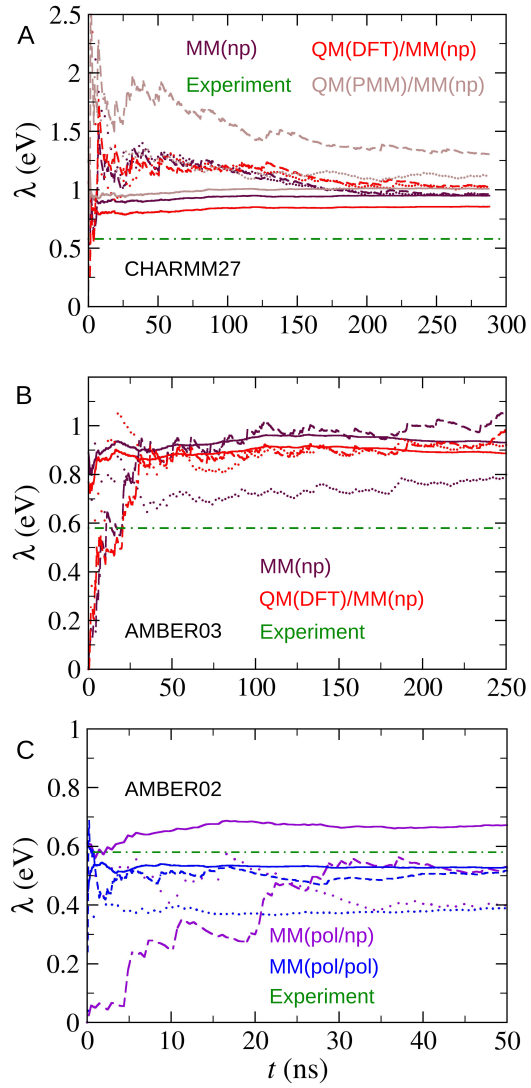

Figure 4: Accumulating average of reorganization free energies for oxidation of solvated cytochrome c for different computational models and force fields. The Stokes reorganization free energy, λ^{st} (Eq. 3), is shown in solid lines, and the variance reorganization free energies, $\lambda_{\mathrm{R}}^{\mathrm{var}}$ and $\lambda_{\mathrm{O}}^{\mathrm{var}}$ (Eq. 4), in dotted and dashed lines, respectively. In (A) energy gap calculations at the MM(np), QM(DFT)/MM(np) and QM(PMM)/MM(np) level are carried out for MD trajectories obtained with the CHARMM27 protein force field and TIP3P water. In QM/MM calculations QM model 2 is used, np stands for electronically non-polarizable. In (B) energy gap calculations at the MM(np) and QM(DFT)/MM(np) are carried out for configurations from MD trajectories obtained with the AMBER03 protein force field and TIP3P water. In QM/MM calculations QM model 1 is used. In (C) MM(pol/np) calculations are presented where the energy gap is calculated with the polarizable AMBER02 force field and POL3 water on configurations obtained from MD simulation with the AMBER03 protein force field and TIP3P water. In MM(pol/pol) both energy gap and MD simulations are carried out with the AMBER02 force field and POL3 water. See Table 1 for numerical values. Experimental reorganization free energy from electrochemistry is shown in green.[71] See Table 1 for numerical values.

References

(1) Marcus, R. A. On the theory of oxidation-reduction reactions involving electron transfer.I. *J. Chem. Phys.* **1956**, *24*, 966–978.

(2) Marcus, R. A. Electrostatic free energy and other properties of states having nonequilibrium polarization. I. *J. Chem. Phys.* **1956**, *24*, 979–989.

(3) Newton, M. D.; Sutin, N. Electron transfer reactions in condensed phases. *Annu. Rev. Phys. Chem.* **1984**, *35*, 437–480.

(4) Newton, M. D. Quantum chemical probes of electron-transfer kinetics: the nature of donor-acceptor interactions. *Chem. Rev.* **1991**, *91*, 767–792.

(5) Bixon, M.; Jortner, J. Electron transfer - from isolated molecules to biomolecules. *Adv. Chem. Phys.* **1999**, *106*, 35–202.

(6) Newton, M. D. Control of electron transfer kinetics: models for medium reorganization and donor-acceptor coupling. *Adv. Chem. Phys.* **1999**, *106*, 303–375.

(7) Marcus, R. A.; Sutin, N. Electron transfers in chemistry and biology. *Biochim. Biophys. Acta* **1985**, *811*, 265–322.

(8) Moser, C. C.; Keske, J. M.; Warncke, K.; Farid, R. S.; Dutton, P. L. Nature of biological electron transfer. *Nature* **1992**, *355*, 796–802.

(9) Page, C. C.; Moser, C. C.; Chen, X.; Dutton, P. L. Natural engineering principles of electron tunnelling in biological oxidation-reduction. *Nature* **1999**, *402*, 47–52.

(10) Gray, H. B.; Winkler, J. R. Electron tunneling through proteins. *Quart. Rev. Biophys.* **2003**, *36*, 341–372.

(11) Beratan, D. N.; Skourtis, S. S.; Balabin, I. A.; Balaeff, A.; Keinan, S.; Venkatramani, R.; Xiao, D. Steering electrons on moving pathways. *Acc. Chem. Res.* **2009**, *42*, 1669–1678.

(12) Skourtis, S. S.; Waldeck, D. H.; Beratan, D. N. Fluctuations in biological and bioinspired electron-transfer reactions. *Annu. Rev. Phys. Chem.* **2010**, *61*, 461–485.

(13) Venkatramani, R.; Keinan, S.; Balaeff, A.; Beratan, D. N. Nucleic acid charge transfer: black, white and gray. *Coord. Chem. Rev.* **2011**, *255*, 635–648.

(14) Saen-Oon, S.; M, F. L.; Guallar, V. Electron transfer in proteins: theory, applications and future perspectives. *Phys. Chem. Chem. Phys.* **2013**, *15*, 15271–15285.

(15) Kubař, T.; Elstner, M. A hybrid approach to simulation of electron transfer in complex molecular systems. *J. R. Soc. Interface* **2013**, *10*, 20130415.

(16) Matyushov, D. V. Protein electron transfer: dynamics and statistics. *J. Chem. Phys.* **2013**, *139*, 025102.

(17) Skourtis, S. S. In *Electron Transfer in Proteins*; Masoud Mohseni, G. S. E., Yasser Omar, Plenio, M. B., Eds.; Cambridge University Press, 2014; Chapter 9, pp 198–217.

(18) Winkler, J. R.; Gray, H. B. Electron flow through metalloproteins. *Chem. Rev.* **2014**, *114*, 3369–3380.

(19) Beratan, D. N.; Liu, C.; Migliore, A.; Polizzi, N. F.; Skourtis, S. S.; Zhang, P.; Zhang, Y. Charge transfer in dynamical biosystems, or the treachery of (static) images. *Acc. Chem. Res.* **2015**, *48*, 474–481.

(20) Narth, C.; Gillet, N.; Cailliez, F.; Levy, B.; de la Lande, A. Electron transfer, decoherence, and protein dynamics: insights from atomistic simulations. *Acc. Chem. Res.* **2015**, *48*, 1090–1097.

(21) de la Lande, A.; Gillet, N.; Chen, S.; Salahub, D. R. Progress and challenges in simulating and understanding electron transfer in proteins. *Arch. Biochem. Biophys.* **2015**, *582*, 28–41.

(22) Blumberger, J. Free energies for biological electron transfer from QM/MM calculation: method, application and critical assessment. *Phys. Chem. Chem. Phys.* **2008**, *10*, 5651–5667.

(23) Blumberger, J. Recent advances in the theory and molecular simulation of biological electron transfer reactions. *Chem. Rev.* **2015**, *115*, 11191–11238.

(24) Jiang, X.; Futera, Z.; Ali, M. E.; Gajdos, F.; Rudorff, G. F. v.; Carof, A.; Breuer, M.; Blumberger, J. Cysteine linkages accelerate electron flow through tetra-heme protein STC. *J. Am. Chem. Soc.* **2017**, *139*, 17237–17240.

(25) Jiang, Y.; Geng, H.; Li, W.; Shuai, Z. Understanding carrier transport in organic semiconductors: computation of charge mobility considering quantum nuclear tunneling and delocalization effects. *J. Chem. Theor. Comput.* **2019**, *15*, 1477–1491.

(26) El-Naggar, M. Y.; Wanger, G.; Leung, K.; Yuzvinsky, T. D.; Southam, G.; Yang, J.; Lau, W. M.; Nealson, K. H.; Gorby, Y. A. Electrical transport along bacterial nanowires from Shewanella oneidensis MR-1. *Proc. Natl. Acad. Sci. USA* **2010**, *107*, 18127–18131.

(27) Pirbadian, S.; El-Naggar, M. Y. Multistep hopping and extracellular charge transfer in microbial redox chains. *Phys. Chem. Chem. Phys.* **2012**, *14*, 13802–13808.

(28) Subramanian, P.; Pirbadian, S.; El-Naggar, M. Y.; Jensen, G. J. Ultrastructure of Shewanella oneidensis MR-1 nanowires revealed by electron cryotomography. *Proc. Nat. Acad. Sci. USA* **2018**, *115*, E3246–E3255.

(29) Xu, S.; Barrozo, A.; Tender, L. M.; Krylov, A. I.; El-Naggar, M. Y. Multiheme cytochrome mediated redox conduction through Shewanella oneidensis MR-1 cells. *J. Am. Chem. Soc.* **2018**, *140*, 10085–10089.

(30) Chong, G. W.; Karbelkar, A. A.; El-Naggar, M. Y. Natures conductors: what can

microbial multi-heme cytochromes teach us about electron transport and biological energy conversion? *Curr. Opin. Chem. Biol.* **2018**, *47*, 7–17.

(31) Breuer, M.; Rosso, K. M.; Blumberger, J.; Butt, J. N. Multi-heme cytochromes in Shewanella oneidensis MR-1: structures, functions and opportuntities. *J. R. Soc. Interface* **2015**, *12*, 20141117.

(32) Yates, M. D.; Golden, J. P.; Roy, J.; Strycharz-Glaven, S. M.; Tsoi, S.; Erickson, J. S.; El-Naggar, M. Y.; Bartone, S. C.; Tender, L. M. Thermally activated long range electron transport in living biofilms. *Phys. Chem. Chem. Phys.* **2015**, *17*, 32564–32570.

(33) Yates, M. D.; Eddie, B. J.; Kotloski, N. J.; Lebedev, N.; Malanoski, A. P.; Lin, B.; Strycharz-Glaven, S. M.; Tender, L. M. Toward understanding long-distance extracellular electron transport in an electroautotrophic microbial community. *Energy Environ. Sci.* **2016**, *9*, 3544–3558.

(34) Rosso, K. M.; Dupuis, M. Reorganization energy associated with small polaron mobility in iron oxide. *J. Chem. Phys.* **2004**, *120*, 7050–7054.

(35) Alexandrov, V.; Rosso, K. M. Electron transport in pure and substituted iron oxyhydroxides by small-polaron migration. *J. Chem. Phys.* **2014**, *140*, 234701.

(36) McKenna, K.; Blumberger, J. Crossover from incoherent to coherent electron tunneling between defects in MgO. *Phys. Rev. B* **2012**, *86*, 245110.

(37) Blumberger, J.; McKenna, K. Constrained density functional theory applied to electron tunnelling between defects in MgO. *Phys. Chem. Chem. Phys.* **2013**, *15*, 2184–2196.

(38) Coropceanu, V.; Cornil, J.; da Silva, D. A.; Olivier, Y.; Silbey, R.; Bredas, J.-L. Charge transport in organic semiconductors. *Chem. Rev.* **2007**, *107*, 926–952.

(39) Nelson, J.; Kwiatkowski, J. J.; Kirkpatrick, J.; Frost, J. M. Modeling charge transport in organic photovoltaic materials. *Acc. Chem. Res.* **2009**, *42*, 1768–1778.

(40) Oberhofer, H.; Reuter, K.; Blumberger, J. Charge transport in molecular materials: an assessment of computational methods. *Chem. Rev.* **2017**, *117*, 10319–10357.

(41) Giannini, S.; Carof, A.; Blumberger, J. Crossover from hopping to band-like charge transport in an organic semiconductor model: atomistic non-adiabatic molecular dynamics simulation. *J. Phys. Chem. Lett.* **2018**, *9*, 3116–3123.

(42) Marcus, R. A. On theory of electron-transfer reactions. VI. Unified treatment for homogeneous and electrode reactions. *J. Chem. Phys.* **1965**, *43*, 679.

(43) Chidsey, C. E. D. Free-energy and temperature-dependence of electron-transfer at the metal-electrolyte interface. *Science* **1991**, *251*, 919–922.

(44) Nitzan, A. *Chemical dynamics in condensed phases*; Oxford University Press, 2006.

(45) Futera, Z.; Blumberger, J. Electronic couplings for charge transfer across molecule/metal and molecule/semiconductor interfaces: performance of the projector operator-based diabatization approach. *J. Phys. Chem. C* **2017**, *121*, 19677–19689.

(46) Zusman, L. D. Outer-sphere electron transfer in polar solvents. *Chem. Phys.* **1980**, *49*, 295–304.

(47) Warshel, A. Dynamics of reactions in polar solvents. Semiclassical trajectory studies of electron-transfer and proton-transfer reactions. *J. Phys. Chem.* **1982**, *86*, 2218–2224.

(48) Small, D. W.; Matyushov, D. V.; Voth, G. A. The theory of electron transfer reactions: What may be missing? *J. Am. Chem. Soc.* **2003**, *125*, 7470–7478.

(49) Blumberger, J. Cu^{+}_{aq}/Cu^{2+}_{aq} redox reaction exhibits strong nonlinear solvent response due to change in coordination number. *J. Am. Chem. Soc.* **2008**, *130*, 16065–16068.

(50) LeBard, D. N.; Matyushov, D. V. Protein-water electrostatics and principles of bioenergetics. *Phys. Chem. Chem. Phys.* **2010**, *12*, 15335–15348.

(51) Vuilleumier, R.; Tay, K. A.; Jeanmairet, G.; Borgis, D.; Boutin, A. Extension of Marcus picture for electron transfer reactions with large solvation changes. *J. Am. Chem. Soc.* **2012**, *134*, 2067–2074.

(52) Amadei, A.; Daidone, I.; Bortolotti, C. A. A general statistical mechanical approach for modeling redox thermodynamics: the reaction and reorganization free energies. *RSC Adv.* **2013**, *3*, 19657–19665.

(53) Daidone, I.; Amadei, A.; Zaccanti, F.; Borsari, M.; Bortolotti, C. A. How the reorganization free energy affects the reduction potential of structurally homologous cytochromes. *J. Phys. Chem. Lett.* **2014**, *5*, 1534–1540.

(54) Sumi, H.; Marcus, R. A. Dynamical effects in electron transfer reactions. *J. Chem. Phys.* **1986**, *84*, 4894–4914.

(55) Matyushov, D. Protein electron transfer: is biology (thermo)dynamic? *J. Phys. Condens. Matter* **2015**, *27*, 473001.

(56) Carter, E. A.; Hynes, J. T. Solute-dependent solvent force constants for ion pairs and neutral pairs in a polar solvent. *J. Phys. Chem.* **1989**, *93*, 2184–2187.

(57) LeBard, D. N.; Kapko, V.; Matyushov, D. V. Energetics and kinetics of primary charge separation in bacterial photosynthesis. *J. Phys. Chem. B* **2008**, *112*, 10322–10342.

(58) LeBard, D. N.; Matyushov, D. V. Energetics of bacterial photosynthesis. *J. Phys. Chem. B* **2009**, *113*, 12424–12437.

(59) Blumberger, J.; Tavernelli, I.; Klein, M. L.; Sprik, M. Diabatic free energy curves and coordination fluctuations for the aqueous Ag^{+}/Ag^{2+} redox couple: A biased Born-Oppenheimer molecular dynamics investigation. *J. Chem. Phys.* **2006**, *124*, 064507.

(60) LeBard, D. N.; Matyushov, D. V. Ferroelectric hydration shells around proteins: electrostatics of the protein-water interface. *J. Phys. Chem. B* **2010**, *114*, 9246–9258.

(61) Dinpajooh, M.; Martin, D. R.; Matyushov, D. V. Polarizability of the active site of cytochrome c reduces the activation barrier for electron transfer. *Sci. Rep.* **2016**, *6*, 28152.

(62) Seyedi, S. S.; Waskasi, M. M.; Matyushov, D. V. Theory and electrochemistry of cytochrome c. *J. Phys. Chem. B* **2017**, *121*, 4958–4967.

(63) Seyedi, S.; Matyushov, D. V. Termination of biological function at low temperatures: glass or structural transition? *J. Phys. Chem. Lett.* **2018**, *9*, 2359–2366.

(64) Tipmanee, V.; Oberhofer, H.; Park, M.; Kim, K. S.; Blumberger, J. Prediction of reorganization free energies for biological electron transfer: a comparative study of Ru-modified cytochromes and a 4-helix bundle protein. *J. Am. Chem. Soc.* **2010**, *132*, 17032–17040.

(65) Breuer, M.; Zarzycki, P.; Shi, L.; Clarke, T. A.; Edwards, M.; Butt, J.; Richardson, D. J.; Fredrickson, J. K.; Zachara, J. M.; Blumberger, J. et al. Molecular structure and free energy landscape for electron transport in the deca-Heme cytochrome MtrF. *Biochem. Soc. Trans.* **2012**, *40*, 1198–1203.

(66) Tipmanee, V.; Blumberger, J. Kinetics of the terminal electron transfer step in cytochrome c oxidase. *J. Phys. Chem. B* **2012**, *116*, 1876–1883.

(67) Blumberger, J.; Klein, M. L. Reorganization free energies for long-range electron transfer in a porphyrin-binding four-helix bundle protein. *J. Am. Chem. Soc.* **2006**, *128*, 13854–13867.

(68) Aschi, M.; Spezia, R.; Nola, A. D.; Amadei, A. A first-principles method to model perturbed electronic wavefunctions: the effect of an external homogeneous electric field. *Chem. Phys. Lett.* **2001**, *344*, 374–380.

(69) Bortolotti, C. A.; Amadei, A.; Aschi, M.; Borsari, M.; Corni, S.; Sola, M.; Daidone, I. The reversible opening of water channels in cytochrome c modulates the heme iron reduction potential. *J. Am. Chem. Soc.* **2012**, *134*, 13670–13678.

(70) Zanetti-Polzi, L.; Galdo, S. D.; Daidone, I.; D'Abramo, M.; Barone, V.; Aschi, M.; Amadei, A. Extending the perturbed matrix method beyond the dipolar approximation: comparison of different levels of theory. *Phys. Chem. Chem. Phys.* **2018**, *20*, 24369–24378.

(71) Terrettaz, S.; Cheng, J.; Miller, C. J.; Guiles, R. D. Kinetic parameters for cytochrome c via insulated electrode voltammetry. *J. Am. Chem. Soc.* **1996**, *118*, 7857–7858.

(72) Wei, J. J.; Liu, H.; Niki, K.; Margoliash, E.; Waldeck, D. H. Probing electron tunneling pathways: electrochemical study of rat heart cytochrome c and its mutant on pyridine-terminated SAMs. *J. Phys. Chem. B* **2004**, *108*, 16912–16917.

(73) Banci, L.; Bertini, I.; Huber, J. G.; Spyroulias, G. A.; Turano, P. Solution structure of reduced horse heart cytochrome c. *J. Biol. Inorg. Chem.* **1999**, *4*, 21–31.

(74) Louie, G. V.; Brayer, G. D. High-resolution refinement of yeast iso-1-cytochrome c and comparisons with other eukaryotic cytochromes c. *J. Mol. Biol.* **1990**, *214*, 527–555.

(75) Feller, S. E.; Mackerell, A. D. An improved empirical potential energy function for molecular simulations of phospholipids. *J. Phys. Chem. B* **2000**, *104*, 7510–7515.

(76) Kaszuba, K. D.; Postila, P. A.; Cramariuc, O.; Sarewicz, M.; Osyczka, A.; Vattulainen, I.; Rg, T. Parameterization of the prosthetic redox centers of the bacterial cytochrome bc 1 complex for atomistic molecular dynamics simulations. *Theor. Chem. Acc.* **2013**, *132*, 1370.

(77) Case, D. A.; Betz, R. M.; Cerutti, D. S.; T. E. Cheatham, I.; Darden, T. A.; Duke, R. E.;

Giese, T. J.; Gohlke, H.; Goetz, A. W.; Homeyer, N. *et al.*; AMBER16, Version 16, University of California, San Francisco, 2016.

(78) Breuer, M.; Zarzycki, P.; Blumberger, J.; Rosso, K. M. Thermodynamics of electron flow in the bacterial deca-heme cytochrome MtrF. *J. Am. Chem. Soc.* **2012**, *134*, 9868–9871.

(79) Humphrey, W.; Dalke, A.; Schulten, K. VMD - Visual Molecular Dynamics. *J. Molec. Graphics* **1996**, *14*, 33–38.

(80) Phillips, J. C.; Braun, R.; Wang, W.; Gumbart, J.; Tajkhorshid, E.; Villa, E.; Chipot, C.; Skeel, R. D.; Kale, L.; Schulten, K. Scalable molecular dynamics with NAMD. *J. Comput. Chem.* **2005**, *26*, 1781–1802.

(81) Hutter, J.; Iannuzzi, M.; Schiffmann, F.; VandeVondele, J. CP2K: atomistic simulations of condensed matter systems. *WIREs Comput Mol Sci* **2014**, *4*, 15–25.

(82) Perdew, J. P.; Burke, K.; Ernzerhof, M. Generalized gradient approximation made simple. *Phys. Rev. Lett.* **1996**, *77*, 3865–3868.

(83) Goedecker, S.; Teter, M.; Hutter, J. Separable dual-space Gaussian pseudopotentials. *Phys. Rev. B* **1996**, *54*, 1703–1710.

(84) Gao, J.; Amara, P.; Alhambra, C.; Field, M. J. A generalized hybrid orbital (GHO) method for the treatment of boundary atoms in combined QM/MM calculations. *J Phys Chem A* **1998**, *102*, 4714–4721.

(85) Frisch, M. J.; Trucks, G. W.; Schlegel, H. B.; Scuseria, G. E.; Robb, M. A.; Cheeseman, J. R.; Scalmani, G.; Barone, V.; Petersson, G. A.; Nakatsuji, H. *et al.*; Gaussian 16, Revision B.01, Gaussian Inc., Wallingford, CT, 2016.

(86) Caldwell, J. W.; Kollman, P. A. Structure and properties of neat liquids using nonadditive molecular dynamics: water, methanol, and N-methylacetamide. *J. Phys. Chem.* **1995**, *99*, 6208–6219.

(87) Blumberger, J.; Lamoureux, G. Reorganization free energies and quantum corrections for a model electron self-exchange reaction: comparison of polarizable and non-polarizable solvent models. *Mol. Phys.* **2008**, *106*, 1597–1611.

(88) Seidel, R.; Faubel, M.; Winter, B.; Blumberger, J. Single-ion reorganization free energy of aqueous $Ru(bpy)_3^{2+/3+}$ and $Ru(H_2O)_6^{2+/3+}$ from photoemission spectroscopy and density functional molecular dynamics simulation. *J. Am. Chem. Soc.* **2009**, *131*, 16127–16137.

(89) Oberhofer, H.; Blumberger, J. Insight into the mechanism of the Ru^{2+}-Ru^{3+} electron self-exchange reaction from quantitative rate calculations. *Angew. Chem. Int. Ed.* **2010**, *49*, 3631–3634.

(90) Moens, J.; Seidel, R.; Geerlings, P.; Faubel, M.; Winter, B.; Blumberger, J. Energy levels and redox properties of aqueous $Mn^{2+/3+}$ from photoemission spectroscopy and density functional molecular dynamics simulation. *J. Phys. Chem. B* **2010**, *114*, 9173–9182.

(91) Seidel, R.; Thurmer, S.; Moens, J.; Geerlings, P.; Blumberger, J.; Winter, B. Valence photoemission spectra of aqueous $Fe^{2+/3+}$ and $[Fe(CN)_6]^{4-/3-}$ and their interpretation by DFT calculations. *J. Phys. Chem. B* **2011**, *115*, 11671–11677.

(92) Gupta, S.; Matyushov, D. V. Effects of solvent and solute polarizability on the reorganization energy of electron transfer. *J. Phys. Chem. A* **2004**, *108*, 2087–2096.

(93) Dinpajooh, M.; Newton, M. D.; Matyushov, D. V. Free energy functionals for polarization fluctuations: Pekar factor revisited. *J. Chem. Phys.* **2017**, *146*, 064504.

(94) Muegge, I.; Qi, P. X.; Wand, A. J.; Chu, Z. T.; Warshel, A. The reorganization energy of cytochrome c revisited. *J. Phys. Chem. B* **1997**, *101*, 825–836.

(95) Ren, P.; Ponder, J. W. Polarizable atomic multipole water model for molecular mechanics simulation. *J. Phys. Chem. B* **2003**, *107*, 5933–5947.

(96) Lehmann, E. L.; Casella, G. *Theory of point estimation*; Spinger-Verlag: New York, 1998.

Graphical TOC Entry

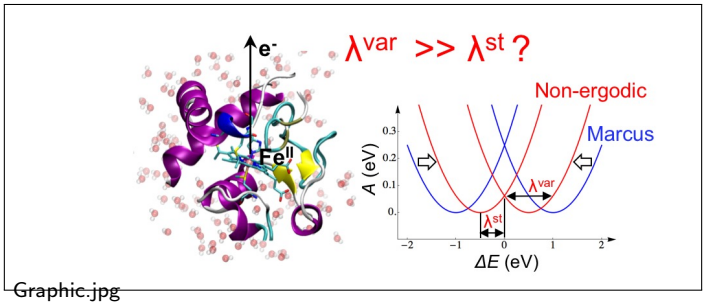

Graphic.jpg